Proceedings of the 9th World Congress on New Technologies (NewTech'23)
Brunel University, London, United Kingdom - August 09-11, 2023
Paper No. ICNFA 126
DOI: 10.11159/icnfa23.126

Manipulating Bubble Dynamics and Heat Transfer using 3D Superbiphilic Micro/Nanostructures

Christopher Salmean1[1], Huihe Qiu[1,2]
[1]Department of Mechanical and Aerospace Engineering,
The Hong Kong University of Science and Technology,
Clear Water Bay, Kowloon, Hong Kong SAR, China
c.salmean@connect.ust.hk; meqiu@ust.hk

[2]Sustainable Energy and Environment Thrust,
The Hong Kong University of Science and Technology (Guangzhou),
Nansha, Guangzhou, China 511453
meqiu@ust.hk

Abstract **-** With the development and miniaturization of high density integrated circuits and multi-functions of electronic chips, the heat flux generated by the chips has been greatly increased, which becomes a bottleneck for further development. Therefore, it is emergent to develop new and efficient thermal management techniques for electronics cooling. Phase change heat transfer, such as boiling and evaporation, is a promising technique for the cooling of electronic devices. However, the prevention of vapor film formation is a fundamental challenge for the enhancement of phase change systems, and an impetus therefore exists for the discovery of new techniques to segregate nucleation during their formation. It has been shown that the surface of the three-dimensional superbiphilic wettability patterns can control the bubble dynamics and phase transition process of the three-phase contact line, thereby greatly enhancing the heat transfer coefficient and critical heat flux of pool boiling and flow boiling with a range of geometries, orientations and morphologies in order to influence the surface-tension forces which resist the bubble's departure and wicking performance. Previous study also found that the concentration Marangoni effect using low-boiling-point multi-component working fluids may help further improve heat transfer performance. Therefore, it is of great interests to study the multiphase flow, wicking performance, heat and mass transfer and contact line dynamics on the three-dimensional superbiphilic wettability patterned surfaces. This talk will present our recently progresses in novel three-dimensional superbiphilic wettability patterns for enhancing phase change heat transfer and how to manipulate the liquid propagation coefficient using non-uniform micropillar array. The experimental results utilizing high speed visualization and time-resolved PIV systems will be presented.

Keywords**:** Superbiphilic Micro/Nanostructures; Contact-line pinning; Wettability patterning; Bubble dynamics; Silicon nanograss

1. Introduction

Recent studies into the possibility of heat transfer enhancement using heterogeneous wettability [1-5] have aimed to capture the benefits of biphilic surfaces through combination of hydrophobic patches, which provide preferential nucleation sites with low energy requirements for bubble nucleation, with a surrounding hydrophilic network which can deliver coolant to hotspots and hinder bubble spreading. However, there is still a limit to the capabilities of two-dimensional boiling surfaces. Contact-line manipulation appears to be a useful technique to expedite bubble departure, but the balance between the surface tension and hydrodynamic forces has a fundamental limit due to the extremely superhydrophobic nucleation sites needed to ensure strong pinning. In this paper, we will demonstrate a technique to further affect the force balance through manipulation of the hydrodynamic forces acting upon forming bubbles.

An as-of-yet unexplored aspect of wettability patterning is the manipulation of contact line morphology in order to increase the hydrodynamic forces acting upon a bubble. In this paper, new concept is demonstrated, where flow boiling heat transfer properties are enhanced through the deliberate utilisation of contact-line pinning on 3-dimensional (3D) micro/nanostructured surfaces with extreme wetting contrasts. Two mechanisms are probed:

(i) the formation and subsequent pinning of bubbles atop symmetrically superbiphilic (SsBPi) micropillar arrays using superhydrophobic (sHPo) nanostructures. Bubble generation atop micropillars increases the encountered drag and lift forces due to the higher velocity of impinging liquid, and the relocation of vapour generation away from the channel base increases the rewetting potential;

(ii) the orientation of sHPo patches on either the upstream- or downstream- facing surfaces of a micropillar (denoted by u-Janus and d-Janus, respectively) to manipulate bubble coalescence characteristics. The interplay of drag forces and bubble pinning is used to limit coalescence, which can increase both the heat transfer coefficient and maximum sustainable heat flux.

Both mechanisms rely upon strong contact line pinning using nanostructures with tuned wettability and show improved performance over the homogeneous sHPo and superhydrophilic (sHPi) pillar arrays which were tested as control experiments.

The directional control of bubble formation using anisotropic micro/nanostructures is applied in a flow boiling setting, where drag forces are critical for bubble dynamics and boiling properties. Moving the contact-line manipulation into 3 dimensions allows the harnessing of hydrodynamic forces in the direction normal to the hydrophobic patches rather than flowing across them, which is an important change of convention when compared to any 2-dimensional studies. We foresee that the utilisation of drag for control of bubble dynamics might be of interest to future researchers as new fabrication technologies become more widespread. Ultimately, this work may inspire new designs of engineered micro/nanostructured surfaces in 3 dimensions, as heat transfer requirements are increasingly met using 3D-printed, integrated microchannels or monolithic heat exchangers, and the manipulation of bubble dynamics in 3D becomes increasingly achievable.

2. Materials and Methods

2.1. Chip design

It was decided to use in-line pillars (i.e., a square array) in this study. The present study desired to examine the possibility of manipulation of neighbouring bubble pairs, and for the neighbouring bubbles in the u-Janus and d-Janus cases to stretch perpendicular to the flow direction during their pairwise merging phase. In this configuration, the greatest drag forces would be experienced by bubbles, while the pressure drop in single-phase regions were expected to be small [6,7].

Micropillar height was chosen using the theoretical bounds of fin efficiency and heat transfer. As the heat transfer coefficient in this study was calculated using the lumped capacitance model, it is important to ensure that the heat transfer remains convection-dominated in even the 'worst-case' scenario, meaning that the Biot number should ideally remain at around 0.1 when the fin temperature is around 150 °C (the maximum foreseeable temperature in the experiments) [8]. Using the equation for characteristic length ($L_c=V/A_{surf}$) and taking 1 MW/m^{2}K as the maximum foreseeable heat transfer coefficient, a height/radius ratio may be determined at which these conditions are met (Figure 1). An asymptote is encountered at around 18 μm micropillar radius, below which there is no solution which allows the lumped capacitance model to be used at HTC of 1 MW/m^{2}K. We therefore rounded to 20 μm micropillar radius, which allowed the lumped capacitance model to be used in the modelling of micropillars shorter than 52.3 μm. For this reason, micropillar arrays with heights of 50 μm, 25 μm and 4 μm were tested in this study.

2.2. Device fabrication

The proposed boiling enhancement mechanisms were probed using photolithography and thin-film techniques. Silicon chips were fabricated with integrated heating and sensing electronics on their backsides and hierarchical wettability patterns and nano/microstructures on their frontsides. The heating/sensing platform was fabricated, but the frontside (boiling) surfaces were patterned with 3-dimensional wettability patterns on hierarchical micro/nanostructures as described in the following section. Figure 2 shows a full process flow for this study.

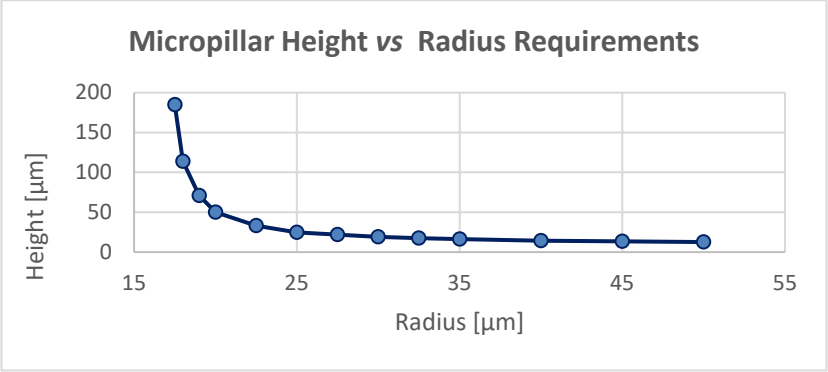

Figure 1: Maximum micropillar height at which Biot number is below 0.1 for each radius, at temperature of 150 ° C and HTC of 1 MW/m^{2}K.

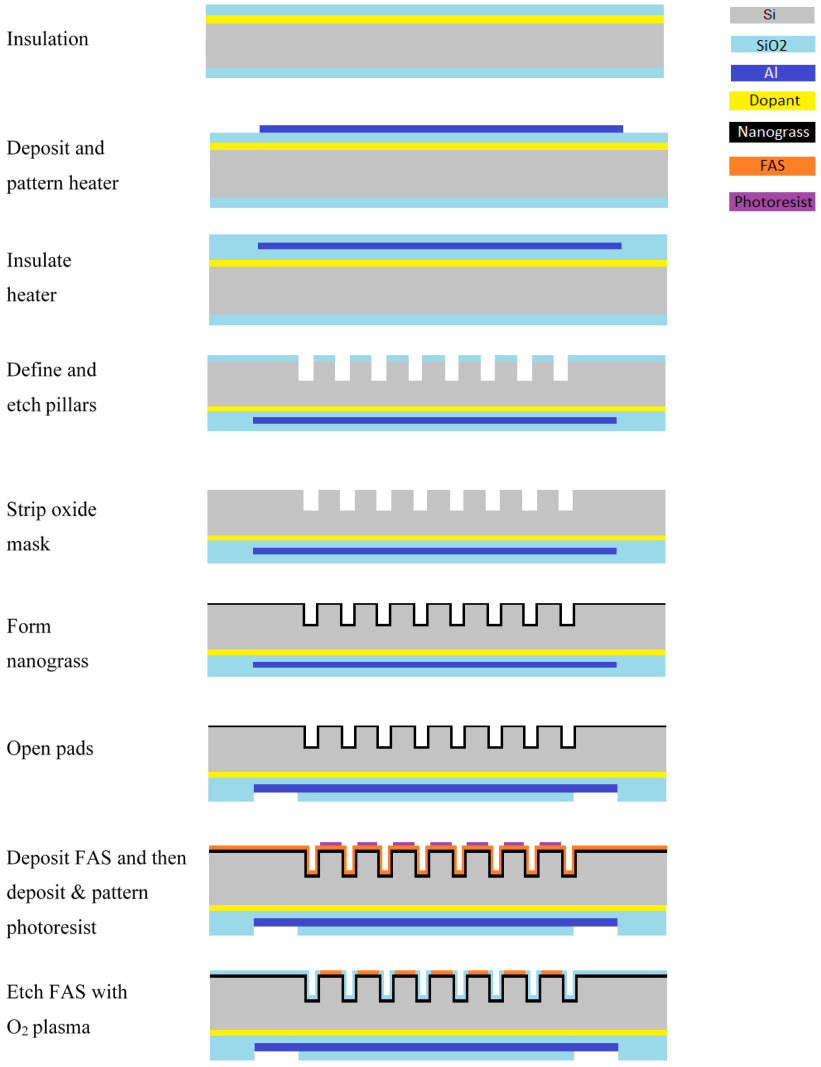

Figure 2: Process flow schematic for the fabrication of hierarchical superbiphilic micro/nanostructures.

The micropillars were defined on the wafer's frontside using the backside alignment function of the SUSS MA-6 mask aligner (SUSS MicroTec, Germany) to match the backside heaters and frontside boiling areas. Reactive-ion etching was performed to strip the SiO2 from the desired etching areas, and highly-anisotropic DRIE was employed to etch pillars with the desired height (Omega Rapier XE, SPTS, UK). In this study, micropillar arrays with heights of 4 µm, 25 µm and 50 µm (Figure 3 (a-c), respectively), pillar diameter of 40 µm and square pitch of 160 µm were patterned on the boiling surface. The remaining SiO_2 and photoresist were then stripped from the wafer's frontside, and unmasked anisotropic etching with $SF6/O_2$ was used to create a uniform nanograss with height of 0.8-2.0 µm (Omega Rapier XE, SPTS, UK) ((Figure 3 (d)). Buffered hydrofluoric acid solution was then employed to open up the backside electrical pads. The wettability patterns were created by first hydrophobising the entire wafer and then selectively hydrophilising specific areas. In both cases, spray coating was employed due to the tendency for photoresist to bead and roll off of the superhydrophobic wafer rather than form a film. An additional advantage of this coating method was that it could be used for conformal coating of the micropillar arrays, and it was therefore possible to employ the exact same recipes for wettability patterning of the 3D micro/nanostructures. The measured static contact angles in this study were 171 ° on the superhydrophobic nanograss ((Figure 3 (e)), and ~3 ° on the superhydrophilic nanograss ((Figure 3 (f)). A schematic overview of the designed wettability patterns is shown in (Figure 3 (g).

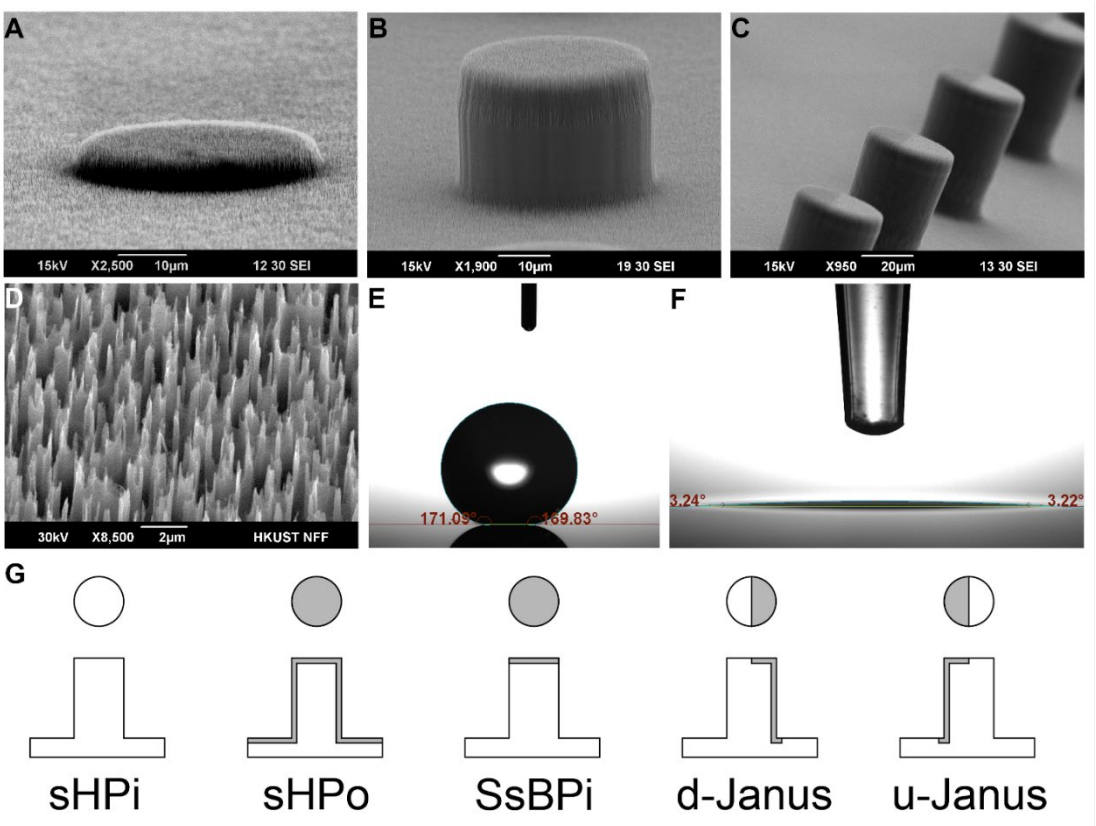

Figure 3: (a-c) SEM images of representative micropillars with respective heights of 4 µm, 25 µm and 50 µm; (d) representative SEM image of the silicon nanograss; optical tensiometer measurement of the static contact angles of water on (e) superhydrophobic and (f) superhydrophilic surfaces; (g) schematics showing the side- and top-views of each designed wettability, with the shaded regions representing superhydrophobic surfaces. The upstream direction is to the left of the diagram.

2.3. Experiments

The microgap channels (depth 230 μm plus micropillar height, width 2 mm, length 20 mm) were installed in a flow loop and supplied with degassed, deionised water at 2 ml/min. Heating was achieved using five aluminium film microheaters in series, the linear resistance-temperature relationships of which were calibrated to infer the average temperature at five locations inside the microchannel.

The experimental procedure in this study was as the following. Prior to use, deionised water is partially degassed in a separate chamber by holding under vacuum for several hours. Before charging the flow loop, the stainless-steel reservoir is allowed to heat up and the entire loop is then evacuated. The high temperature and vacuum conditions of the liquid reservoir cause the water to boil vigorously during charging, thereby completing the degassing process. The reservoir is then returned to atmospheric pressure and heated to saturation temperature to prevent re-absorption of non-condensable gases.

During experiments, all experimental data were collected using an automated testing procedure in which the electrical power provided to the chip was incremented upwards in approximately uniform steps, and a burst of 60 temperature, pressure and power measurements were taken over the course of 1 minute once the system was deemed to have reached steady state for each step. Steady state was defined as the point where the outlet fluid temperature and pump pressure deviated by less than ±1 % in any 5-minute period. Each experiment was continued until a temperature of 140 °C was measured anywhere on the chip, at which point the experiment was stopped; at higher temperatures, we observed degradation of the FAS monolayer and of the polymeric materials used during packaging (namely the epoxy sealant and PET spacer). In this study, we refer to this point as the maximum sustainable heat flux (MSHF), due to uncertainty around the exact point of CHF.

2.4. Results and Discussion

To quantify the effects of the various nucleation and departure regimes, the heat flux was plotted against wall temperature (Figure 4(a)) and boiling heat transfer coefficient (Figure 4(b)). On the homogeneous microstructures, the expected trends were observed; sHPo micropillars reached MSHF shortly after the onset of boiling, and sHPi micropillars achieved comparatively higher heat fluxes in all cases (Figure 4(a)). It is known that the relative swiftness of vapour film formation and consequent burnout within the nanostructures depends upon wettability, with sHPo surfaces exhibiting an extreme resistance to rewetting and propensity to form a stable vapour film. A quasi-annular flow regime is engendered thereon, thus limiting heat transfer as shown in Figure 4(b) and generating large wall superheat. Contrastingly, the sHPi surfaces exhibited a higher peak HTC at all micropillar heights, as their nucleation sites were sparser but emitted a steady stream of bubbles.

Focusing on the biphilic micropillar arrays, the SsBPi design has a comparable MSHF to the sHPi case (Figure 4(a)) but exhibits lower superheats across a range of heat fluxes in the two taller micropillar arrays. Superhydrophobic patches may be activated at lower temperatures than sHPi areas, so (at intermediate heat flux) we observed the nucleation of bubbles on the sHPo pillartops of the SsBPi micropillars rather than in the hotter sHPi areas near the micropillars' bases. The SsBPi micropillars do not obstruct neighbouring bubbles from touching, so bubbles are similarly prone to merging at all heights- however, high wall superheat was only seen in the 4 μm case, which we suspect to be due to the raising of nucleation sites away from the microchannel wall. Retention of a thick liquid sublayer beneath the plane of bubble coalescence reduced wall superheat through additional availability of latent heat and consequent inhibition of hotspot spreading, and the formation of bubbles closer to the microchannel's horizontal midplane- and subsequent increase of drag forces from impinging flow- contributes towards improved HTC on taller micropillars.

The d-Janus micropillars reached higher MSHF than the other designs at all heights. We attribute this to the unique orientation of the sHPo nucleation sites relative to the flow direction. On both anisotropic designs, the taller Janus micropillars act as a barrier to coalescence in the flow-wise direction, while the unique orientation of the bubbles prevents widespread merging from occurring. It was expected that the HTC would be improved in the heterogeneous cases due to the greatly increased number of nucleation sites and extension of the contact line as

bubbles become pinned to the biphilic interface[106]- an expectation that was borne out by the observed results (Figure 4(b)). The maximum HTC was recorded on the 50 µm d-Janus micropillar array (87.6 ± 20.6 kW/m^{2}K at 462.5 ± 2.7 kW/m^2), representing an improvement of 95% and 90% over the 50 µm sHPi and sHPo analogues, respectively.

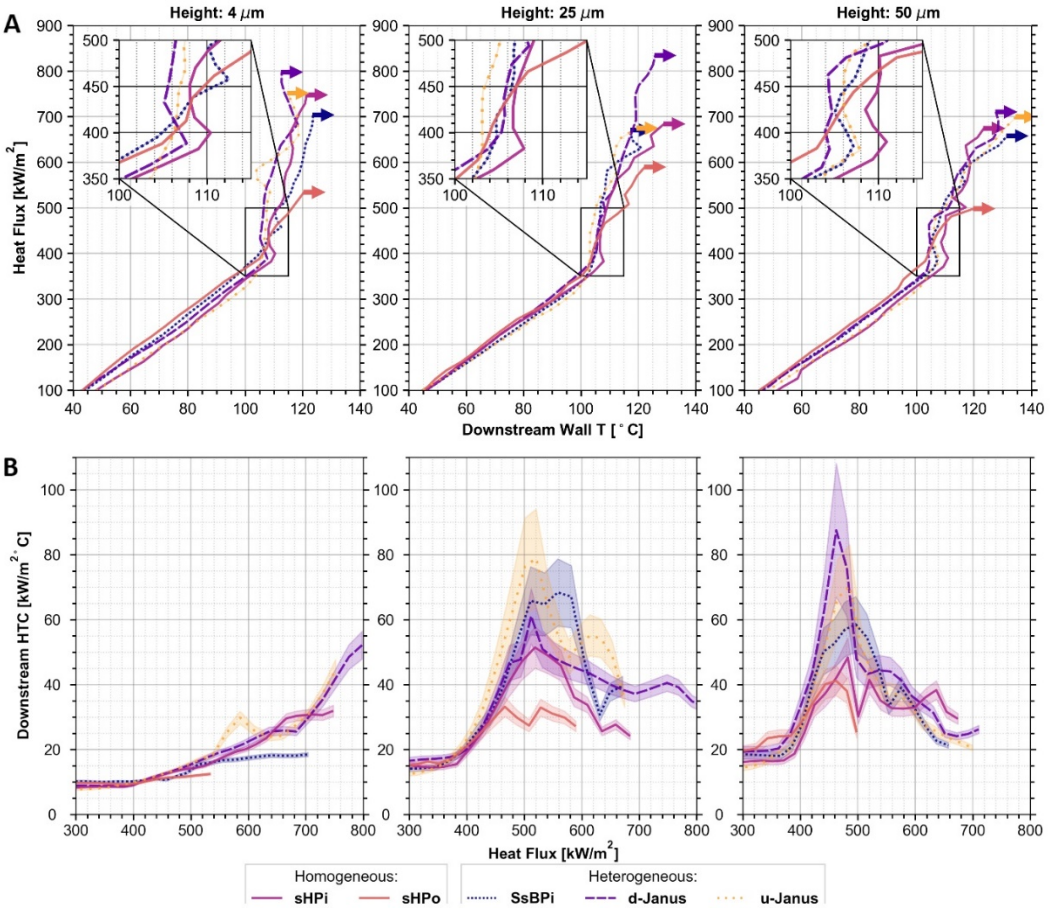

Figure 4: (a) Boiling curves and (b) boiling heat transfer coefficients for each chip design. Each measurement is calculated for the downstream-most heaters, i.e., between 8-10 mm of heated length. Each curve represents the interpolated average for at least three experimental runs (interpolated in 25 Wcm^{-2} increments). Shaded regions calculated from propagation of error are shown bounding the curves.

The quantitative HTC improvements for the biphilic designs in Figure 4 can be understood through analysis of the forces on generated bubbles. Contact line pinning at the biphilic interfaces may first be assessed by approximating the balance between capillary and viscous forces within the nanograss[116]. Usually, imbibition is largest on the inter-microstructural scale, but wettability patterning eliminates this component through contact line pinning, thus making the nanograss capillary forces the primary source of spreading. The calculations show that by approximating the nanograss as an array of square nanopillars, the capillary forces for water in the hydrophobic and hydrophilic nanograss may be quantified. The contact angle hysteresis (CAH) and contact line length are critical components of vapour slug pinning, so the very small contact area and CAH in the Cassie regime allows us to ignore these forces for bubbles passing over a sHPi surface. This is illustrated in Figure 5, wherein the passing vapour slug only touches the pillartops of the SsBPi surface. As the vapour slug is pushed forwards, it is intuitive

that the variation of wetted area is altered only in the newly- covered and newly- uncovered areas at the leading and trailing edges of the bubble.

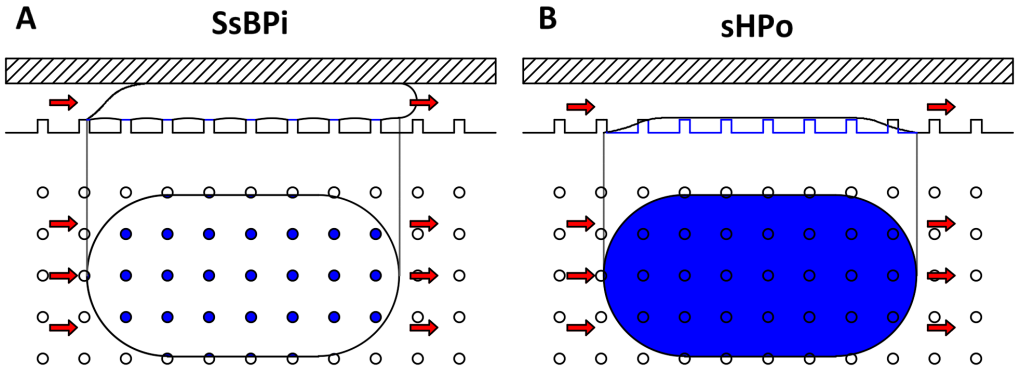

Figure 5: Side-view and top-view illustrations of wetted areas during slug flow in (a) SsBPi and (b) sHPo case. Blue areas are wetted, and red arrows indicate the direction of travel of the vapour slug.

3. Conclusion

In summary, we demonstrated that the expansion of bubble pinning into 3 dimensions offers a host of possibilities for the control of bubble departure characteristics and consequent improvement of heat transfer properties. Of the wide selection of possible configurations, we showed that the HTC and CHF of microchannel flow boiling can be enhanced using numerous designs which exploit the interplay of drag and surface tension forces. As a result, 81% and 113% higher boiling HTCs were realised on asymmetrical 3D biphilic micro/nanostructures when compared to homogeneously superhydrophilic and superhydrophobic equivalents, respectively. We theorise that the use of nanograss in this study strongly pins the contact line, which can be used to alter the hydrodynamic properties surrounding the bubble and thereby assist in the removal of vapour from the channel wall.

The directional control of bubble formation using anisotropic microstructures is applied in a flow boiling setting, where drag forces are critical for bubble dynamics and boiling properties. Moving the contact-line manipulation into 3 dimensions allows the harnessing of hydrodynamic forces in the direction normal to the hydrophobic patches rather than flowing across them, which is an important change of convention when compared to any 2-dimensional studies. The primary benefit of this paradigm is the further alteration of the force balances, through creation of additional drag forces when compared to a 2-dimensional configuration.

We foresee that the utilisation of drag for control of bubble dynamics might be of interest to future researchers as new fabrication technologies become more widespread. Ultimately, this work may inspire new designs of engineered surfaces in 3 dimensions, as heat transfer requirements in (for example) rocket engines, nuclear reactors and electrical circuits are increasingly met using 3D-printed, integrated microchannels or monolithic heat exchangers, and the manipulation of bubble dynamics in 3D becomes increasingly achievable. The possible applications for this work also extend outside of thermal engineering, with additional opportunities arising in electrolysis and chemical reaction engineering due to the engineered movement of bubbles to influence their hydrodynamic interactions.

Acknowledgements

This work was supported by the Research Grants Council (RGC) of the Government of Hong Kong Special Administrative Region (HKSAR) with RGC/GRF Project No. 16205018, the International Science and Technology Project of Huangpu District of Guangzhou City (2020GH08) and RGC Hong Kong Ph.D. Fellowship Scheme. We also wish to acknowledge the Nanosystem Fabrication Facility (CWB) of the Hong Kong University of Science and Technology for their expertise during device design and fabrication.

References

[1] X. Chen, H. Wang, C. Salmean, M. Mei, Y. Wang, H.H. Qiu, "Distinct Features of Chemically Patterned Surfaces for Boiling Heat Transfer Enhancement," *Advances in Heat Transfer*; Elsevier, 2022; vol. 54, pp 241–288.

[2] H. Jo, D. I. Yu, H. Noh, H. S. Park, M. H. Kim, "Boiling on Spatially Controlled Heterogeneous Surfaces: Wettability Patterns on Microstructures," *Applied Physics Letters* 2015, 106, 181602.

[3] A. R. Betz, J. Jenkins, C. J. Kim, D. Attinger, "Boiling Heat Transfer on Superhydrophilic, Superhydrophobic, and Superbiphilic Surfaces," *International Journal of Heat and Mass Transfer* 2013, 57 (2), 733–741.

[4] X. Chen, H.H. Qiu, "Bubble Dynamics and Heat Transfer on a Wettability Patterned Surface," *International Journal of Heat and Mass Transfer* 2015, 88, 544–551.

[5] A. R. Betz, J. Xu, H.H. Qiu, D. Attinger, "Do Surfaces with Mixed Hydrophilic and Hydrophobic Areas Enhance Pool Boiling?" *Applied Physics Letters* 2010, 97 (14), 1–4.

[6] S. V. Jadhav, P. M. Pawar, "Performance Analysis of Microchannel with Different Pin Fin Layouts," *International Journal of Numerical Modelling: Electronic Networks, Devices and Fields* 2020, 33 (2), 1–19.

[7] O. N. Sara, "Performance Analysis of Rectangular Ducts with Staggered Square Pin Fins," *Energy Conversion and Management* 2003, 44, 1787–1803.

[8] F. P. Incropera, D. P. DeWitt, T. L. Bergman, A. S. Lavine, "*Fundamentals of Heat and Mass Transfer*," 6. ed.; Wiley: Singapore, 2013.